



## Mantle plumes: Dynamic models and seismic images

**L. Boschi**

*Eidgenössische Technische Hochschule Hönggerberg, Institute of Geophysics, Schafmattstr. 30, 8093 Zurich, Switzerland  
(lapo@erdw.ethz.ch)*

**T. W. Becker**

*Department of Earth Sciences, University of Southern California, MC 0740, ZHS269, 3651 Trousdale Parkway,  
Los Angeles, California 90089-0740, USA*

**B. Steinberger**

*Center for Geodynamics, Norges Geologiske Undersøkelse, Leiv Eirikssons vei 39, N-7491 Trondheim, Norway*

[1] Different theories on the origin of hot spots have been debated for a long time by many authors from different fields, and global-scale seismic tomography is probably the most effective tool at our disposal to substantiate, modify, or abandon the mantle-plume hypothesis. We attempt to identify coherent, approximately vertical slow/hot anomalies in recently published maps of P and S velocity heterogeneity throughout the mantle, combining the following independent quantitative approaches: (1) development and application of a “plume-detection” algorithm, which allows us to identify a variety of vertically coherent features, with similar properties, in all considered tomographic models, and (2) quantification of the similarity between patterns of various tomographic versus dynamic plume-conduit models. Experiment 2 is complicated by the inherent dependence of plume conduit tilt on mantle flow and by the dependence of the latter on the lateral structure of the Earth’s mantle, which can only be extrapolated from seismic tomography itself: it is inherently difficult to disentangle the role of upwellings in “attracting” plumes versus plumes being defined as relatively slow, and thus located in regions of upwellings. Our results favor the idea that only a small subset of known hot spots have a lower-mantle origin. Most of those that do can be associated geographically with a few well-defined slow/hot regions of very large scale in the lowermost mantle. We find evidence for both secondary plumes originating from the mentioned slow/hot regions and deep plumes whose conduits remain narrow all the way to the lowermost mantle. To best agree with tomographic results, modeled plume conduits must take into account the effects of advection and the associated displacement of plume sources at the base of the mantle.

**Components:** 8474 words, 14 figures.

**Keywords:** global seismology; mantle dynamics; mantle plumes; tomography; *P* waves; *S* waves.

**Index Terms:** 7299 Seismology: General or miscellaneous; 8120 Tectonophysics: Dynamics of lithosphere and mantle: general (1213); 7208 Seismology: Mantle (1212, 1213, 8124).

**Received** 22 June 2007; **Accepted** 18 July 2007; **Published** 17 October 2007.

Boschi, L., T. W. Becker, and B. Steinberger (2007), Mantle plumes: Dynamic models and seismic images, *Geochem. Geophys. Geosyst.*, 8, Q10006, doi:10.1029/2007GC001733.

## 1. Introduction

[2] Deep mantle plumes, or localized thermal upwellings originating deep in the Earth's lower mantle, were first invoked by *Morgan* [1971] to explain intraplate volcanism not accounted for by plate tectonics. The plume concept accommodated a variety of observations made at hot spots, including the existence of linear chains of volcanoes with monotonous age progression (the most evident being the one associated with Hawaii), anomalously large values of buoyancy flux with associated topographic swell, and the distinct isotopic signature of volcanic rocks, accordingly dubbed ocean island basalt (OIB) in contrast to mid-ocean ridge basalt (MORB).

[3] *Morgan's* [1971] original model has been challenged or modified by many authors [*Turcotte and Oxburgh*, 1973; *Morgan*, 1978; *Sleep*, 1990, 2002a, 2002b; *Clouard and Bonneville*, 2001; *Gaherty*, 2001; *Montagner and Ritsema*, 2001] and abandoned by some [*Anderson*, 1998, 2000; *Foulger*, 2002; *Foulger et al.*, 2005]. *Anderson* [2000, p. 3623] claims for instance that "deep narrow thermal plumes are unnecessary and precluded by uplift and subsidence data. The locations and volumes of 'midplate' volcanism appear to be controlled by lithospheric architecture, stress and cracks." Other recent studies [e.g., *Davies*, 2005; *Sleep*, 2006] appear to favor the plume hypothesis, while not ruling out other theories. Geodynamic models of the convecting mantle are consistent with mantle upwellings in the form of narrow plumes, provided that a thermal boundary layer exists at the base of the mantle [*Zhong*, 2006]. *Courtilot et al.* [2003] have studied a selection of hot spots from the catalogues compiled by *Davies* [1988], *Sleep* [1990] and *Steinberger* [2000] and found that they could be classified into different groups on the basis of the accompanying sets of surface observations, and the associated seismic velocity anomalies from the global tomographic model of *Ritsema et al.* [1999]; 7 out of 49 analyzed hot spots were found by *Courtilot et al.* [2003] to have likely lower mantle origin.

[4] Evidence from global seismic tomography could be decisive to discriminate between competing theories of hot spot formation [*Nataf*, 2000]. As noted by *Courtilot et al.* [2003], *Ritsema et al.'s* [1999] image of shear-wave velocity in the mantle is slow in regions underlying most hot spots. On the other hand, no truly plume-like velocity anomalies exist in this model: even if available seismic

data had, at least locally, the resolving power to detect narrow upwellings, this power would be lost owing to the long-wavelength parameterization adopted by the authors. Namely, *Ritsema et al.'s* [1999] images are defined horizontally as linear combinations of spherical harmonics up to degree 20, corresponding to a nominal resolution of  $\sim 1000$  km; the diameter of a plume is expected to be locally as small as  $<200$  km [*Nataf*, 2000; *Steinberger and Antretter*, 2006].

[5] Other authors in global tomography have put a special effort in mapping anomalies of lateral extent as limited as possible, making use of globally or locally dense parameterizations [*Grand*, 1994; *van der Hilst et al.*, 1997; *Bijwaard et al.*, 1998; *Simmons et al.*, 2006] and/or relying on improvements in the theoretical formulation of the relationship between seismic data and 3-D Earth structure (finite-frequency versus ray-theory), basis of the tomographic inverse problem [*Ji and Nataf*, 1998a, 1998b; *Montelli et al.*, 2004a, 2004b, 2006b]. Only *Montelli et al.* [2004a, 2004b, 2006b], however, have emphasized the presence, in their models, of plume-like features often extending from lithospheric depths into the lowermost mantle.

[6] The unique character of *Montelli et al.'s* [2004a, 2004b, 2006b] maps is confirmed by *Montelli et al.'s* [2006b] own comparative analysis of recently published tomographic models. One possible explanation is that the finite-frequency approach enhances resolution, making it possible to accurately map anomalies at smaller scales than those imaged so far. The discussion that followed [*de Hoop and van der Hilst*, 2005a, 2005b; *Dahlen and Nolet*, 2005; *van der Hilst and de Hoop*, 2005, 2006; *Boschi*, 2006; *Boschi et al.*, 2006; *Montelli et al.*, 2006a; *Trampert and Spetzler*, 2006] invites one to be more skeptical. One debated issue is the prevalence of *Montelli et al.'s* [2004a, 2004b, 2006b] mapped plume-like features in the upper mantle under ocean islands, where isolated stations are located and, since *Montelli et al.* [2004a, 2004b, 2006b] do not invert surface-wave observations, vertical smearing is then likely [*van der Hilst and de Hoop*, 2005, Figure 5]. Another is the anomalously high average radial coherence of *Montelli et al.'s* [2004a] model at all scale lengths, meaning that not only narrow slow anomalies, but the entire pattern of high- and low-velocity heterogeneities is much smoother, in the vertical direction, than found in any other recent model (see Figure 1 of *Boschi et al.* [2006], which can also be compared with numerous analogous plots of

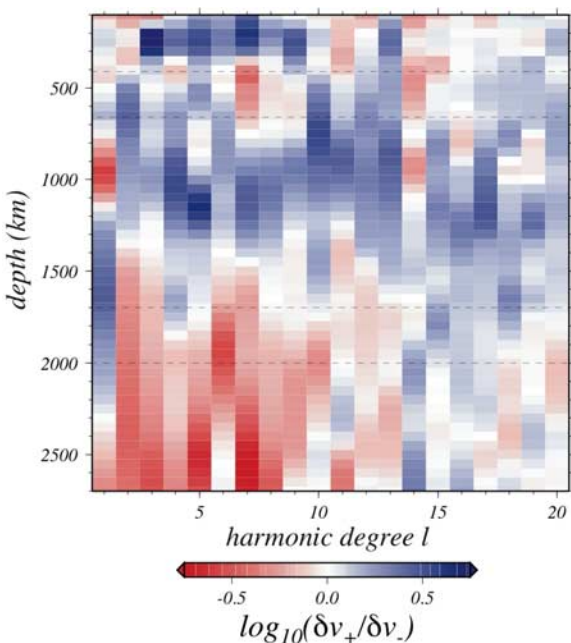


**Figure 1.** We set negative velocity anomalies from model *smean* to zero and compute the harmonic coefficients of the resulting map  $\delta v_+/v$  at a discrete set of depths in the mantle. We likewise compute harmonic coefficients of  $\delta v_-/v$  found after zeroing positive anomalies. We show here the logarithm of the power spectrum [Becker and Boschi, 2002] of  $\delta v_+/\delta v_-$  as a function of depth and harmonic degree  $l$ . Dashed lines mark 410, 660, 1700, and 2000 km depths. Taking the ratio  $\delta v_+/\delta v_-$ , small artifacts that might arise in the decomposition of tomographic models cancel out. In the lower mantle,  $\log_{10}(\delta v_+/\delta v_-) < 0$  at low harmonic degrees, which means that negative velocity anomalies (presumed upwellings of hot material) are generally of larger scale length than positive ones (cold material). The situation is reversed in the midmantle (Reif and Williams, manuscript in preparation, 2007).

Becker and Boschi [2002]). This might reflect the application of a parameterization and/or regularization strategy biased toward vertically homogeneous solutions [Boschi et al., 2006]. Last, the statistical significance of discrepancies between ray-theoretical and finite-frequency solutions of the same inverse problems has been questioned by Trampert and Spetzler [2006].

[7] C. Reif and Q. Williams (The wavelengths of slabs and plumes in the lower mantle: Contrary to the expectations of dynamics?, manuscript in preparation, 2007; hereinafter referred to as Reif and Williams, manuscript in preparation, 2007) attempt to measure the wavelength of the mantle’s seismic structure with a different approach, conducting on

the global tomographic image of C. Reif et al. (Shear and compressional velocity models of the mantle from cluster analysis of long-period waveforms, submitted to *Geophysical Journal International*, 2007) separate spectral analyses of positive and negative seismic velocity anomalies (one might expect that this decomposition of tomographic models can induce artifacts in the power spectra: we verified with a simple synthetic test that such artifacts are negligible). In contrast to expectations from thermal models of mantle convection, negative anomalies turn out to be of systematically longer wavelength in the lowermost mantle. The situation is reversed in the midmantle, where positive anomalies likely associated with subducted slabs are dominant across most of tomographic models’ harmonic spectrum, or the uppermost mantle ( $\leq 300$  km), where fast tectospheric roots are imaged under continents. We analyze model *smean* [Becker and Boschi, 2002] in a similar way (Figure 1), finding consistent results. The dominance of slow structure at long and intermediate wavelengths in the lowermost mantle may be explained by thermochemical heterogeneity. It is not clear whether this is consistent with the absence of seismic detections of a large-scale interface between presumed “piles,” or thermochemical layers [Davaille et al., 2002; Jellinek and Manga, 2002; McNamara and Zhong, 2004, 2005], and the rest of the mantle.

[8] Continuing the earlier work of Montagner [1994], Courtillot et al. [2003], Thorne et al. [2004], and Montelli et al. [2006b], we conduct here a comparison between tomographic models and geodynamic reconstructions of plume shape and location. We first make use of a “plume detector” algorithm (section 2), then quantify the similarities between seismic and dynamic models [Ray and Anderson, 1994; Wen and Anderson, 1997; Seidler et al., 1999; Becker and Boschi, 2002] (section 3). Our reference plume models are based on Steinberger and Antretter’s [2006] (SA06 hereafter) method, accounting for the deflection of plume conduits advected by a convecting mantle. We have applied our analysis to a suite of models from Becker and Boschi’s [2002] database (including, for example, *s20rts*, *bdp00*, *kh00p*, and *pmean*; see Becker and Boschi [2002] for references) finding generally consistent results; here we limit our analysis to a smaller set of *S* and *P* wave velocity models published in the last year, based on updated databases and/or new inversion algorithms: the *S* model of Simmons et al. [2006] (dubbed *tx2007* here), and the *P* and *S* models of

Montelli *et al.* [2006b] (*pri-p05* and *pri-s05*, respectively). We then included models *smean* and *vox3p* for different reasons. *smean* is the *S* model of Becker and Boschi [2002], on which the calculations of plume conduits presented here are based. The similarity between slow anomalies in *smean* and modeled plume conduits (section 3 below) serves as a reference to compare other models against. *vox3p* is a *P*-velocity model that we derived with Boschi and Dziewonski's [1999] method, inverting Antolik *et al.*'s [2001] improved database, as in model *bdp00* [Becker and Boschi, 2002]. *vox3p*, parameterized with 15 layers of 3° equal-area pixels, has higher nominal resolution than *bdp00* (5° equal-area pixels). In most of the mantle, *vox3p* is probably overparameterized, and its high nominal resolution partly damped by our roughness regularization constraint; in well-sampled regions, a grid this dense can describe relatively narrow plumes (i.e., of a few hundred km width [e.g., Zhong *et al.*, 2000; Goes *et al.*, 2004; McNamara and Zhong, 2004; SA06]) should the data be able to resolve them.

## 2. Detection of Plume-Like Anomalies in Tomographic Maps

[9] To detect hot upwellings in a model of seismic velocity, we assume that the relative seismic heterogeneity  $\delta v/v$  is of purely thermal origin. In this approximation, relative temperature (*T*) heterogeneity is simply

$$\delta T/T = -\delta v/v, \quad (1)$$

and no depth-dependent scaling factor between temperature and velocity anomalies needs to be introduced. Denoted  $(\delta T/T)_{\text{mean}}$  and  $(\delta T/T)_{\text{max}}$ , respectively, the mean and maximum values of temperature heterogeneity found at any given depth, we consider *T* at a given location at that depth to be anomalously high if [Labrosse, 2002; Zhong, 2006]

$$\delta T/T > (\delta T/T)_{\text{mean}} + 0.5 \times [(\delta T/T)_{\text{max}} - (\delta T/T)_{\text{mean}}] \quad (2)$$

Once a hot anomaly is identified, we check whether other hot anomalies exist at contiguous grid points within the same layer; the process is iterated, posing no limit to the cumulative horizontal extent of the anomaly. We then search “close” grid points on neighboring layers. We define two grid points belonging to neighboring

layers to be close to each other if they are spaced horizontally by less than  $3 \times$  the vertical spacing in the original model parameterization. In comparison with plume-conduit shape as modeled by SA06, this criterion allows for large plume tilt in the tomographic parameterizations considered here. Plume-like features identified with our detection algorithm do not necessarily conform with the narrower plumes commonly envisioned, such as in the model of SA06. Alternatively, narrow plumes might be embedded in larger slow anomalies.

[10] We run the algorithm once per layer, from 300 km depth (in the shallower part of the upper mantle, slow anomalies associated with mid-oceanic ridges are dominant, and would obscure plume-like features) down to the base of the mantle. Once sets of coherent slow vertical bodies have been identified, we discard those with vertical length less than 700 km (equivalent to 3–4 layers in most tomographic models), and those that are entirely confined to depths larger than 2000 km.

[11] Our plume-detection software is not hardwired to the mentioned parameter values (factor 0.5 in equation (2), lower limit of 700 km for vertical length of slow anomalies, etc.), and we have explored a range of reasonable alternative schemes. The results obtained in various cases do not affect our general conclusions.

[12] It should be noted at this point that equation (2) defines detected plumes as vertically coherent bodies whose seismic velocity is low, at each depth, relative to the surrounding mantle at that depth. This definition is consistent with the reasoning of Seidler *et al.* [1999] and Zhong [2006], with the synthetic results of Goes *et al.* [2004] and SA06, and with typical published seismic images of presumed plumes [e.g., Montelli *et al.*, 2004a].

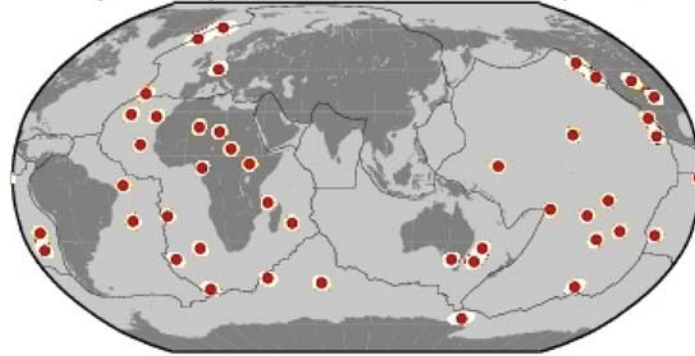
[13] We apply the algorithm to theoretical plume models [SA06] described below (section 3.2.1), and verify that they are properly recovered. The results are shown in Figure 2, accompanied by the following global quantities, useful to quantify the general character of analyzed models:

[14] 1.  $N_P$  is the number of detected plumes; plumes merging at some depths are counted separately as individual plumes.

[15] 2.  $\langle A \rangle$  is the average, over depth, of the percent of solid angle covered by plumes.

[16] 3.  $\Sigma V$  is the total detected plume volume, in percent of total inspected mantle volume (shell comprised between core-mantle boundary and

vertical plumes:  $N_p=40$ ,  $\langle A \rangle=1.95\%$ ,  $\Sigma V=1.85\%$ ,  $\mu=1.05$ ,  $\lambda=1.00$



advected plumes:  $N_p=41$ ,  $\langle A \rangle=1.93\%$ ,  $\Sigma V=1.50\%$ ,  $\mu=1.29$ ,  $\lambda=1.00$

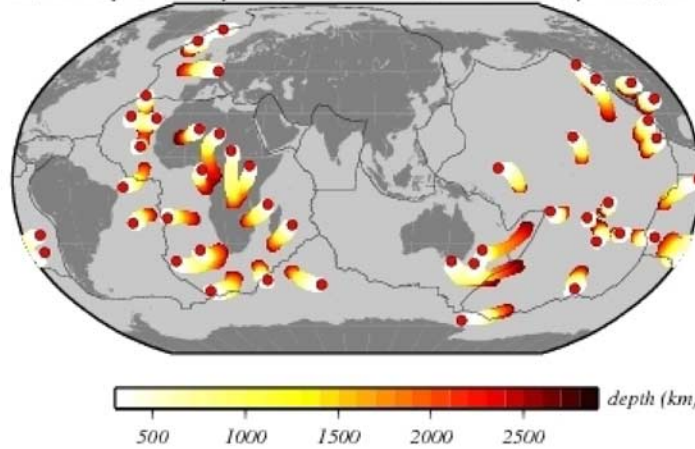


**Figure 2.** Output of our plume-detection algorithm, applied to the (top) vertical-plume and (bottom) advected-plume dynamic models [SA06] discussed in section 3.2.1. Each detected plume extends over a certain range of depths, with patches at different depths distinguished by accordingly different colors.  $\mu > 1$  indicates that a few plumes overlap;  $N_p < 44$  because some plumes are merged over their entire length. These (marginal) effects result from our smoother, spherical harmonic representation (section 3) of the original plume model. Here and in Figures 3 and 4, red circles mark the locations of surface hot spots for which plume conduits were modeled (compare with Figure 6).

300 km depth); the volume occupied by plumes merging at depth is integrated only once.

[17] 4.  $\Sigma V'$  is the cumulative volume of individual, detected plumes, again in percent of inspected mantle volume; merging plumes are counted separately, and their overlapping volume is duplicated.

[18] 5.  $\mu = \Sigma V / \Sigma V'$  is a measure of the overlapping (merging) of distinct plume-like features;  $\mu = 1$  means no plumes merge.

[19] 6.  $\lambda = \Sigma V' / \langle A \rangle$  is a measure of the general vertical extent of detected plume-like features. By construction,  $\lambda = 1$  if all detected plumes extend continuously from the core-mantle boundary to 300 km depth;  $\lambda < 1$  otherwise.

[20] We next apply the algorithm to our selection of  $P$  and  $S$  velocity models, and show the results in Figures 3 and 4, respectively. We provide in Figure 5 a simple statistical analysis of the length of detected plume-like features.

[21] In agreement with, e.g., *Davaille* [1999] and *Courtillot et al.* [2003], it is immediately apparent from all tomographic models that presumed hot upwellings of deep origin are clustered around two broad regions, the southern central Pacific Ocean and Africa with its surrounding oceans, similar to the two “superswells” identified by *Nyblade and Robinson* [1994] and *McNutt* [1998]. Most surface hot spots, particularly those believed to have deep origin [*Courtillot et al.*, 2003], lie within these two regions. In other regions (eastern Asia, North and

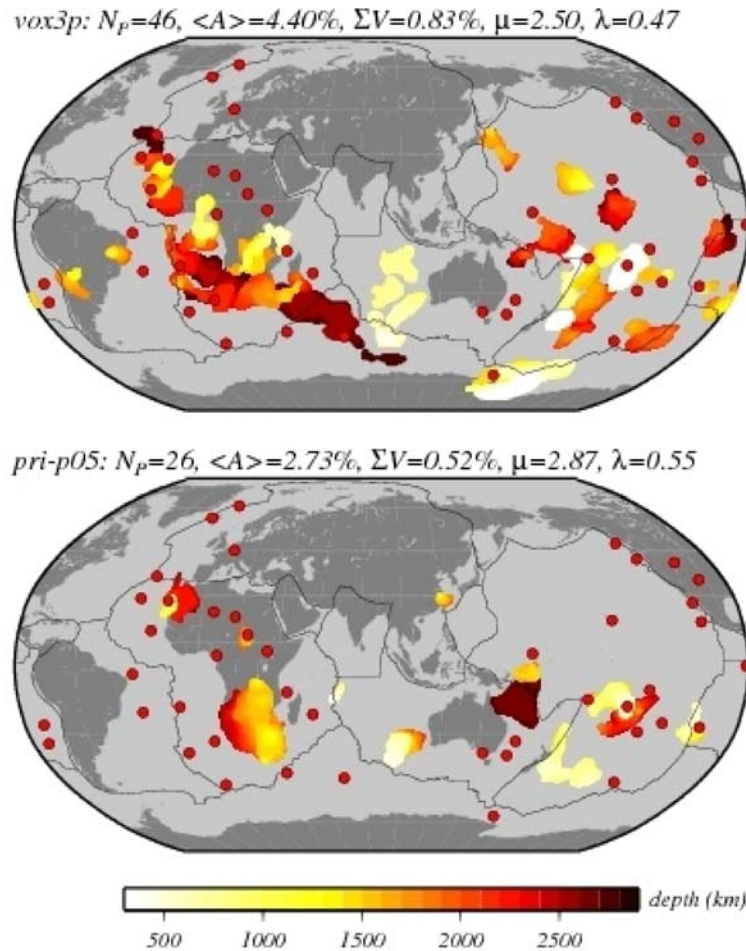


**Figure 3.** Plume-like features detected in the  $P$ -velocity models (top) *vox3p* and (bottom) *pri-p05*. We have verified that some large-scale shallow (yellow-white) features never entirely obscure the deeper continuations of plumes.

South America) we occasionally detect plume-like features of shallower origin.

[22] Within the African superswell, we can perhaps distinguish separate, large-scale slow/hot anomalies where plumes seem to originate: under the Indian Ocean to the southeast of Madagascar; under the southern tip of Africa and the Atlantic Ocean to the southwest of South Africa; under northwestern Africa and the Atlantic Ocean immediately to the west (Canary, Cape Verde). The existence of distinct areas of plume formation at the bottom of the mantle, underneath the same superswell region, was also suggested by Schubert *et al.* [2004].

[23] At large depths, the plume-like features we detect show a long-wavelength pattern, even in models of potentially very high resolution. The most finely parameterized model *vox3p* is characterized

by the highest number ( $N_p=46$ ) of detected plumes. Plume-like features found in lower-resolution models like *smean* are fewer but have a smoother shape, merge more often (higher  $\mu$ ) and occupy a larger volume  $\Sigma V$ . This difference could be explained in terms of limits in tomographic resolution: *vox3p* could be underregularized and contain, as a result, nonphysical oscillations in mapped  $\delta v/v$ , with relatively long-wavelength slow anomalies appearing as groups of disconnected, narrower “plumes”. Conversely, *smean* could be underparameterized (equivalent to overregularized), with narrow features smoothed into large-scale heterogeneities [Schubert *et al.*, 2004]. Both scenarios could take place simultaneously, in differently sampled regions of the mantle. It is impossible at this stage to discriminate between a “plume-forest” (plumes remain separate all through the mantle) [Schubert *et al.*, 2004] and a “plume-farm” (plumes rise

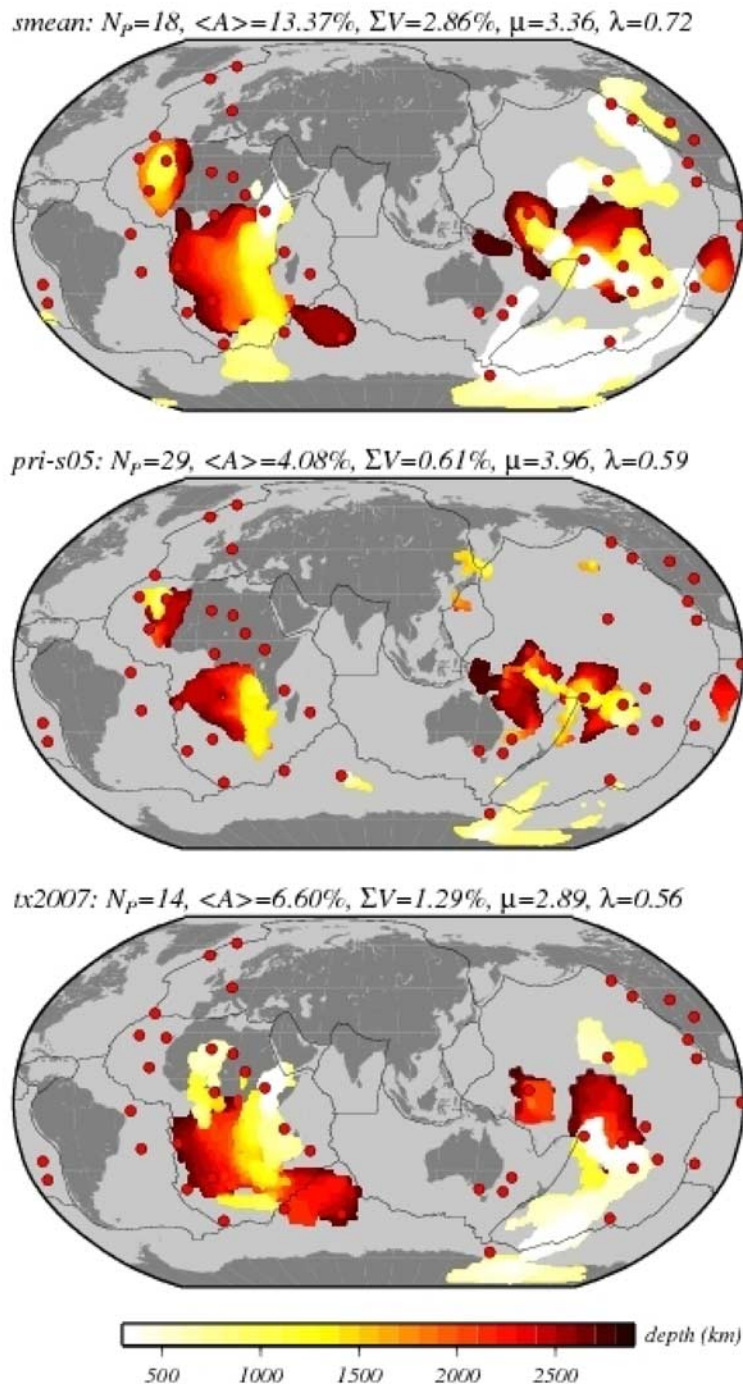


**Figure 4.** Same as Figure 3, for *S*-velocity models (top) *smean*, (middle) *pri-s05*, and (bottom) *tx2007*.

from large-scale hot/slow anomalies) description of mantle upwellings. The geographic correlation between superswells and the lateral distribution of detected plumes, evident from both Figure 3 and Figure 4, remains nonetheless a significant observation.

[24] At shallower depths, presumed plume conduits are narrower and more focused at specific hot spots: see in particular Samoa and Tahiti in all models, East Africa in models *smean* and *tx2007*, Canary in all models with the exception of *tx2007*. Figures 3 and 4 also confirm that models *pri-p05* and *pri-s05* are the most radially coherent ones

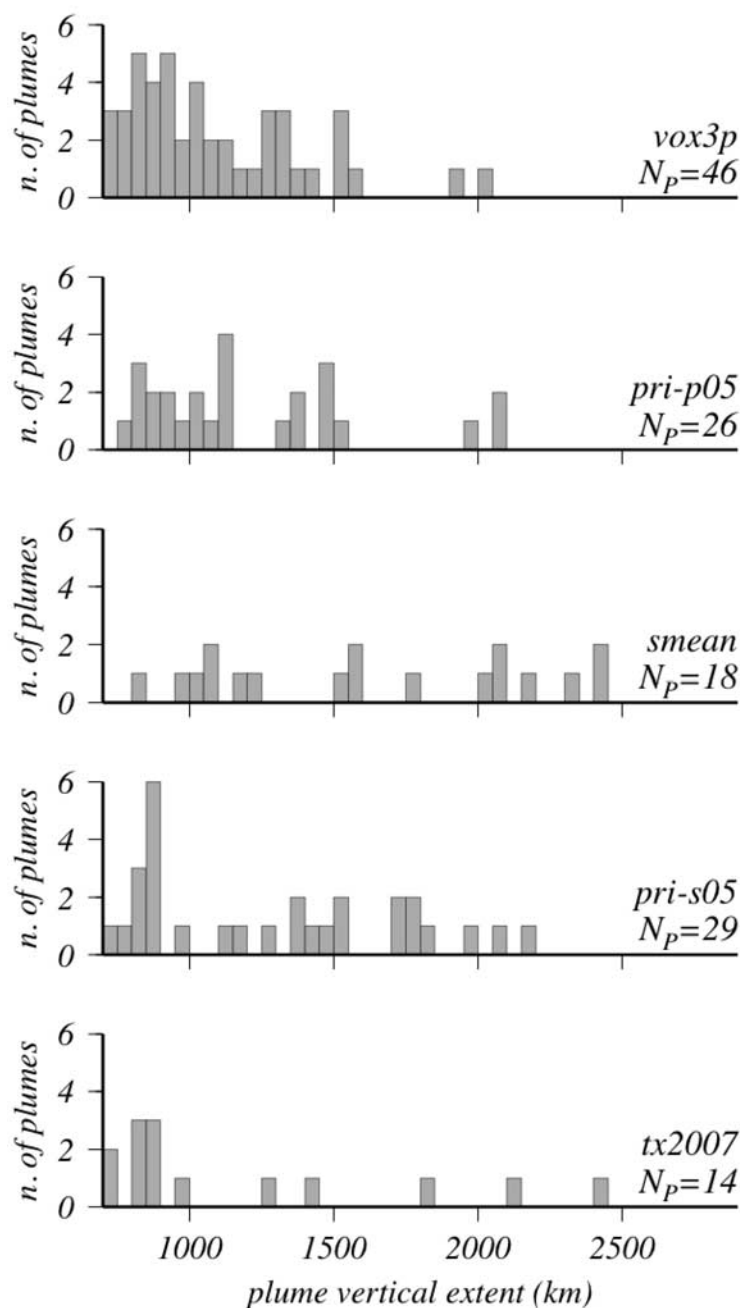


**Figure 5.** Number of detected plumes, from the five *P* and *S* tomographic models in consideration (abbreviation provided on each panel), versus their vertical extent, binned in 50 km intervals. Merging plumes are counted separately: different branches have different length. Detected plumes are most often relatively short, but all models include at least a few plumes extending through most mantle depths, with some exceeding a vertical extent of ~2000 km. The maximum extent our detection algorithm allows for is 2500 km.

[Boschi *et al.*, 2006], with plume-like features generally closer to vertical. Figure 5 shows that the highest average vertical extent of detected plumes (highest  $\lambda$ ) is found from *smean*;  $\lambda$  is smallest for *vox3p* (by construction the roughest

model) and approximately constant ~0.6 for the other models.

[25] Figures 3 through 5 help us to evaluate the global pattern of mapped, vertically coherent slow anomalies. In section 3.3 we shall provide an



estimate of each plume's vertical extent, on the basis of all considered tomographic models.

### 3. Comparison Between Tomographic Images and Geodynamically Modeled Plumes

[26] We next test the interpretation of hot spots in terms of plumes, comparing tomographic models, visually (section 3.1) and quantitatively (sections 3.2.1 and 3.3), with a model of plume conduits as realistic as possible. It is necessary to take into account the advection of plumes by virtue of mantle flow [e.g., *Steinberger and O'Connell*, 1998; *Steinberger*, 2000; SA06]. We apply the method of SA06 to model advected plume conduits associated with the 44 hot spots of Figure 6, complementing the 12 plumes originally modeled by those authors with 32 additional ones. We use the mentioned tomographic model *smean* to establish an a priori map of mantle density structure, governing flow and plume advection. *smean* is a combination [*Becker and Boschi*, 2002] of earlier *S* models by *Grand et al.* [1997], *Masters et al.* [1999], and *Ritsema et al.* [1999]; it has been shown to fit broadband seismic data at least as well [*Qin et al.*, 2007], and geoid observations better [*Steinberger and Calderwood*, 2006] than other recent tomographic models. Because *smean* is an a priori of our modeled plume conduits, it will naturally be more highly correlated with them than other tomographic models. On the basis of the analysis that follows, therefore, no argument can be made that *smean* fits our dynamic model of the Earth's mantle better than other tomographic models. To make such a claim, an independent calculation of flow and advection should be conducted for each tomographic model. Such an exercise is discouraged by earlier studies [e.g., *Steinberger and O'Connell*, 1998; *Steinberger*, 2000; SA06] which indicate that different tomographic models lead to very similar predictions of plume shapes. Here we evaluate, rather, the validity of assumptions that have to be made within the dynamic modeling method (e.g., section 3.2.2).

#### 3.1. Visual Comparison

[27] In Figures 7 and 8, we superimpose the distribution of 12 modeled plume conduits to tomographic *P* and *S* velocity models, respectively. The 12 selected plumes are those of SA06, regarded to have likely deep origin. At each depth, hot spot locations are shown together with the

locations of the corresponding plumes, deflected by mantle flow. While in the midmantle (1200 km) plume locations rarely correspond to clear maxima of slow anomalies, in the upper (300 km) and lowermost (2500 km) mantle the correlation is higher. In the upper mantle it is easy to associate to hot spots a number of slow heterogeneities of very short scale length; this is true in particular of Hawaii, Iceland, Kerguelen, Reunion, Samoa, Tahiti in models *vox3p*, *pri-p05* and *pri-s05*, and of Easter Island in model *pri-s05* only.

[28] In the lowermost mantle, flow-deflected plumes appear to cluster at or in the vicinity of large-scale slow anomalies under southern Africa and southern central Pacific, or the bases of two presumed "superplumes" [*Davaille*, 1999; *Courtillot et al.*, 2003]. Conversely, the corresponding surface hot spot locations often fall in relatively fast regions in most of the lower mantle. Because the shape of SA06's advected plumes is driven by the distribution of hot/slow and fast/cold heterogeneities in the tomographic model *smean*, used as an a priori to model mantle flow, this result is partly expected: upwellings rise from hot regions at the base of the mantle. Figures 7 and 8, however, show that a correlation between plume-shape and slow seismic velocities exists for images of higher resolution than the long-spatial-wavelength pattern of *smean*, with modeled plumes often corresponding to local slow/hot maxima: see, in particular, the two separate slow anomalies beneath southern Africa and the neighboring oceans, where 5 of the 12 major plumes are located, the west coast of northern Africa, the southern central portion of the Pacific Ocean.

[29] High correlations between tomography and dynamic plume models found in the uppermost mantle are likely to be, to some extent, fictitious. *Van der Hilst and de Hoop* [2005] note that some seismic stations are located on ocean islands, right at the top of presumed mantle plumes, and surrounded by seismically undersampled regions; when body-wave data from those stations are included in a tomographic inversion, vertical smearing could result [*Boschi*, 2003], with diffuse, long-wavelength heterogeneities taking a vertically coherent, short-wavelength, plume-like shape. Such speculations do not hold for models that incorporate surface-wave information (only *smean* here), or in the lowermost mantle, where seismic sampling is more uniform: similarities found in that region between *tx2007*, *pri-s05*, *vox3p* and mod-

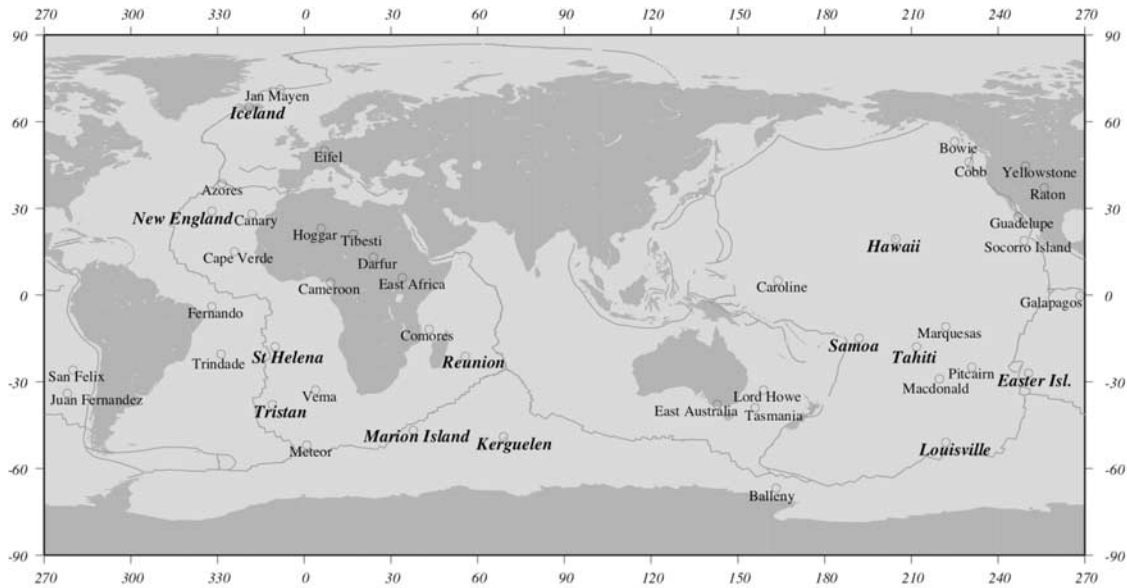


**Figure 6.** Names and locations, as given by Steinberger [2000], of (bold, italic) 12 hot spots of likely deep mantle origin [SA06] and (roman) 32 other hot spots considered separately.

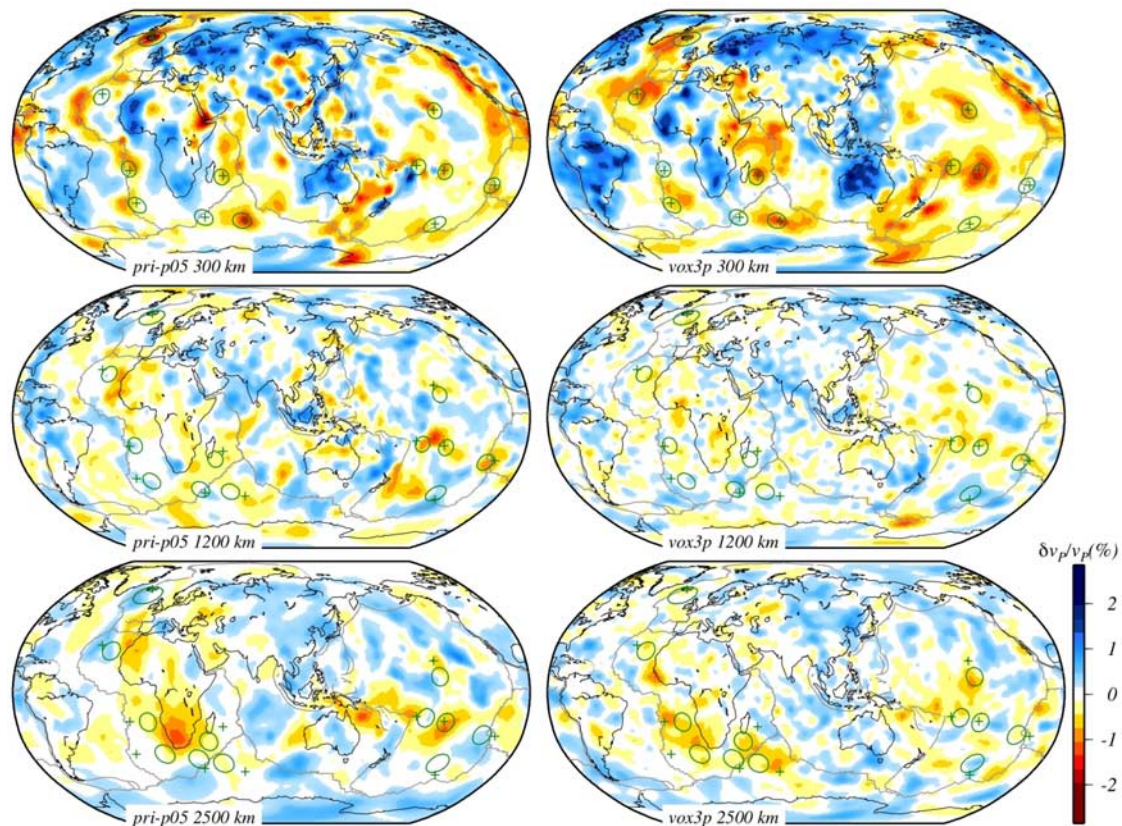


**Figure 7.** *P* models (left) *pri-p05* and (right) *vox3p* compared with SA06’s advected (green circles) and vertical (green crosses) plume locations at (top) 300, (middle) 1200, and (bottom) 2500 km depth.

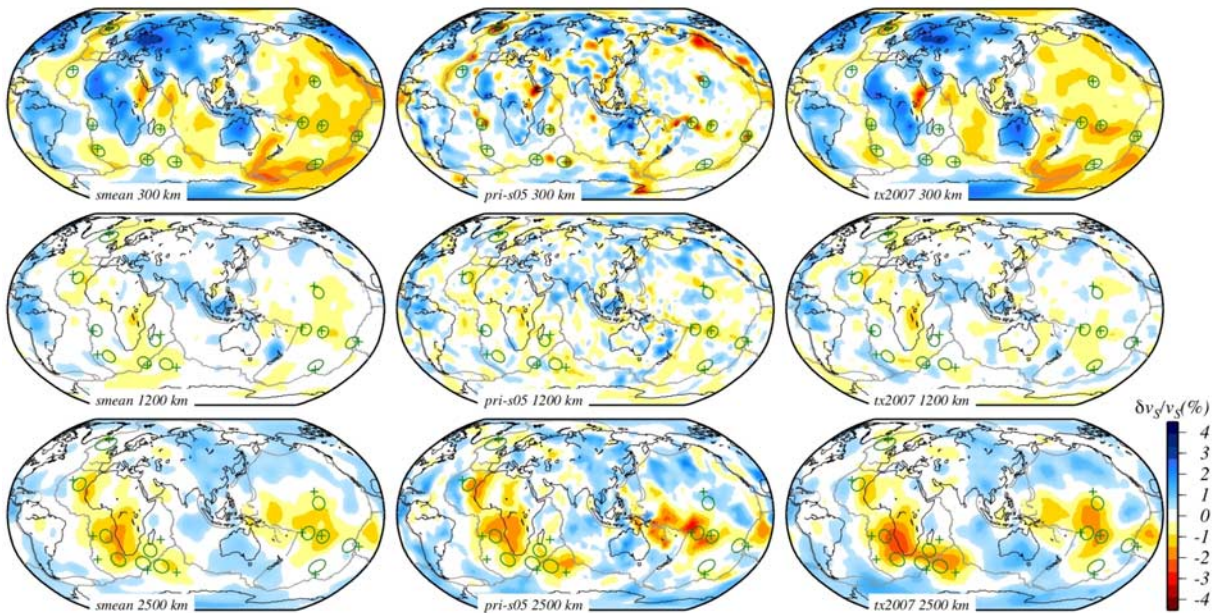


**Figure 8.** Same as Figure 7, for models (left) *smean*, (middle) *pri-s05*, and (right) *tx2007*.

eled deep plumes remain an important result, which we substantiate in the sections that follow.

## 3.2. Correlation Between Seismic Images and Dynamically Modeled Plume Maps

### 3.2.1. Advected and Vertical Plumes

[30] Let us consider two different models of mantle plumes: (1) a dynamic model found applying SA06’s algorithm, in the “moving source” hypothesis, to the 44 hot spot locations in Figure 6 and (2) a model obtained assuming that the locations of the same 44 plumes coincide at all depths with the corresponding surface hot spot locations. Note that advected and vertical plume locations coincide by construction at the Earth’s surface (surface hot spot locations) [SA06].

[31] To implement model 1 we assume the hot spot ages and surface locations of *Steinberger* [2000]. We assign values of anomalous mass fluxes as described by SA06, finding  $10^3$  kg/s for all the 32 hot spots not considered by SA06, with the exceptions of Yellowstone, Macdonald and Marquesas ( $2 \times 10^3$  kg/s). Following SA06, we assume plumes to rise from the top of an assumed low-viscosity layer, at 2620 km depth in the mantle.

[32] For each model, we find the spherical harmonic coefficients (degrees 0 through 63, with a cosine-squared taper applied to avoid ringing) of a

function that equals 1 within 250 km of a (generally depth-dependent) plume location, and 0 elsewhere. We calculate the depth-dependent correlations  $r$ , to maximum harmonic degree 63, between plume models and the patterns of negative velocity heterogeneities from tomographic images, consistently translated into linear combinations of spherical harmonics [*Becker and Boschi, 2002*]. We have verified that the isolation of negative velocity anomalies before spherical harmonic expansion did not introduce any significant artifacts. We show the results of this exercise in Figure 9. Through a Student’s  $t$  test, with the number of harmonics in our expansions  $N = 64^2$ , and the number of degrees of freedom taken to coincide with  $N - 2$ , we find that absolute values of correlation  $|r| > 0.026$  (i.e., most data points in Figure 9) are 90% significant. For a lower number of degrees of freedom, close to more conservative estimates of tomographic resolution (i.e., highest harmonic degree  $\sim 20$ ),  $|r|$  should be  $> 0.079$  for 90% significance.

[33] In agreement with the remarks of section 3.1, velocity anomalies are generally negative within modeled plume conduits, and correlation with the plume models accordingly negative. Figure 9 shows that this effect is stronger for  $S$  than for  $P$  models. Comparison of Figures 9a and 9b shows  $r$  to be systematically higher (larger  $|r|$ , with  $r < 0$ ) when plume advection is taken into account (Figure 9a). To evaluate the statistical significance

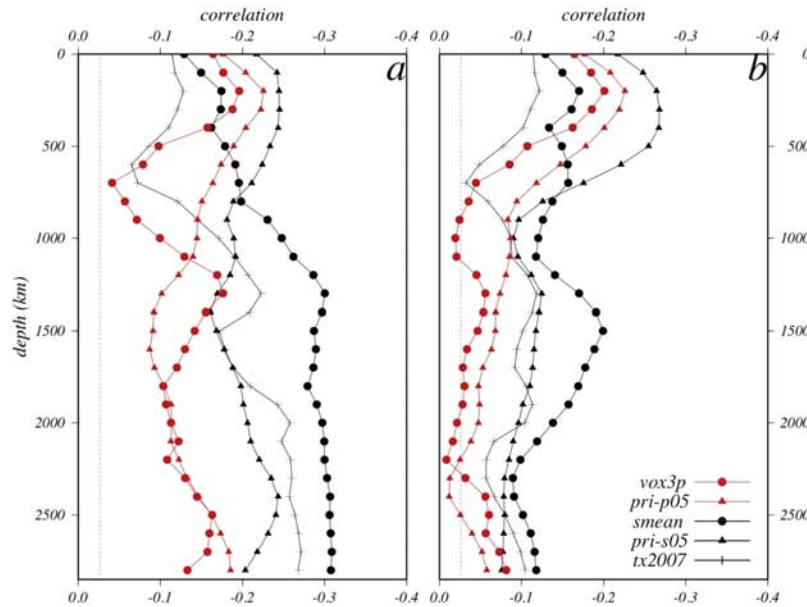


**Figure 9.** Correlations as functions of depth between pattern of negative anomalies from tomographic  $P$  (red lines and symbols) and  $S$  models (black),  $vox3p$  and  $smean$  (circles),  $pri-p05$  and  $pri-s05$  (triangles), and  $tx2007$  (crosses), and (a) 44 advected plume conduits, modeled according to SA06 and (b) the same 44 plumes, assumed vertical under the corresponding hot spots. Dashed, vertical straight lines mark the 90% significance level.

of the latter finding, we first conduct a Fisher's z-transformation [Press *et al.*, 1994] of all found values of  $r$ ,

$$z = \frac{1}{2} \ln \left( \frac{1+r}{1-r} \right). \quad (3)$$

Let us denote  $r_1, r_2$  the values of  $r$  associated, at a certain depth, with a given tomographic model and the advected and vertical plume models, respectively;  $z_1$  and  $z_2$  are found from  $r_1$  and  $r_2$  through equation (3). We find  $z_1$  and  $z_2$  for each considered tomographic model and at each depth, and implement the expression

$$p = 1 - \operatorname{erfc} \left( \frac{|z_1 - z_2|}{\sqrt{2} \sqrt{\frac{1}{N_1-3} + \frac{1}{N_2-3}}} \right) \quad (4)$$

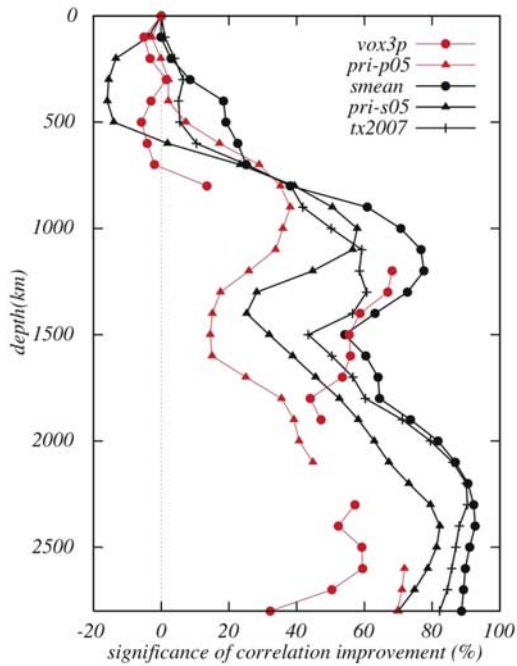
(with  $N_1 = N_2 = N$ ) for the significance of a difference between two measured correlation coefficients  $r_1$  and  $r_2$  [Press *et al.*, 1994].  $p$  can be more intuitively interpreted as the probability that the difference between the two values of correlation  $r_1$  and  $r_2$  be smaller, in the null hypothesis of no true correlation improvement, than the value  $r_1 - r_2$  we have found. The large values of  $p$  resulting from our analysis, shown in

Figure 10, indicate that our account of plume advection introduces a statistically significant improvement in correlation between tomographic and dynamic models, over most of the lower mantle.

[34] Correlations in Figure 9a for  $pri-p05$  and  $pri-s05$  are highest (in absolute value) in the upper mantle, where vertical smearing is more likely (end of section 3.1), and relatively low elsewhere. In the lower mantle, a possible vertical overregularization or underparameterization [Boschi *et al.*, 2006] of  $pri-p05$  and/or  $pri-s05$  could explain the decrease in correlation with modeled plumes, with respect to other considered tomographic models.

### 3.2.2. “Fixed-Source” and “Moving-Source” Plume-Conduit Models

[35] The advected plume-conduit model 1 described above was obtained in the moving-source hypothesis, that is to say, allowing the bases of plume conduits at a depth of 2620 km in the mantle [SA06] to be displaced by mantle flow. The assumption that plume sources move with mantle flow is naturally consistent with the rest of SA06's treatment, and with vigorous convective stirring of



**Figure 10.** Probability  $p$  that  $r_1 - r_2$  in the “null hypothesis” (account of advection does not improve tomographic-dynamic correlation) is less than the value one would find subtracting the curves in Figure 9b from those in Figure 9a. We compute  $p$  according to (equation 4) but multiply it by  $-1$  when vertical plumes are better correlated with tomography than advected ones.  $p$  is left undefined when  $r_1$  and/or  $r_2$  are below the 90% significance level. Symbols and line styles correspond to different tomographic models as in Figure 9.

the lower thermal boundary layer where plumes form.

[36] We next model plume conduits associated with the same 44 surface hot spot locations, with the restriction that their sources are motionless (fixed-source hypothesis). This experiment is based on Davaille *et al.*'s [2002] and Jellinek and Manga's [2002] idea that plumes are formed at thermochemical piles, which in turn help to “anchor” plume sources. While anchored at a fixed origin, plumes are still advected by flow elsewhere in the mantle. We find that the correlation between the resulting fixed-source advected plume-conduit model and tomography is systematically lower than that between model 1 and tomography (Figure 9). With the same procedure followed in section 3.2.1, we determine, and show in Figure 11, the statistical significance  $p$  of said difference in correlation, at a set of closely spaced depths in the mantle. At large depths, where appreciable differences exist be-

tween fixed- and moving-source models,  $p$  is also largest for all considered tomographic models. We conclude that our moving-source plume model 1 fits tomographic results significantly better than its fixed-source counterpart.

[37] This finding is relevant to our understanding of the mechanism of plume formation, with various possible implications. One possibility is that plumes originate from thermochemical “piles” [Tackley, 2002; Davaille *et al.*, 2002; Jellinek and Manga, 2002] at the bottom of the mantle. Jellinek and Manga [2002] hint that chemical piles help fix, or anchor plumes. Our results would then indicate that the latter idea must be reassessed, or that piles are shifted by cold downwellings as suggested by McNamara and Zhong [2004]. Another possibility is that plumes originate from lowermost mantle thermal anomalies, and that such anomalies are displaced by mantle convection [Davaille *et al.*, 2002]. In this scenario, Zhong *et al.* [2000] show that fixed-source and moving-source plumes might co-exist, depending on whether they are formed within or outside of stagnation zones at the core-mantle boundary, or other boundary layers in the mantle.

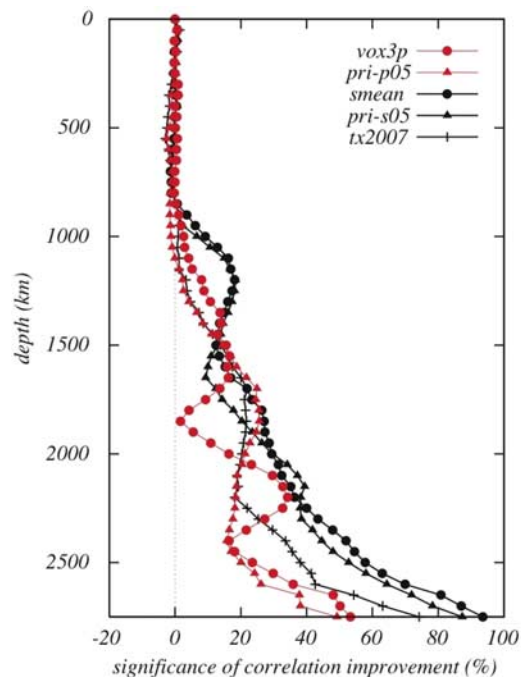


**Figure 11.** Same as Figure 10, but for the correlation improvement achieved by modeling plume conduits in the moving-source versus fixed-source hypothesis.

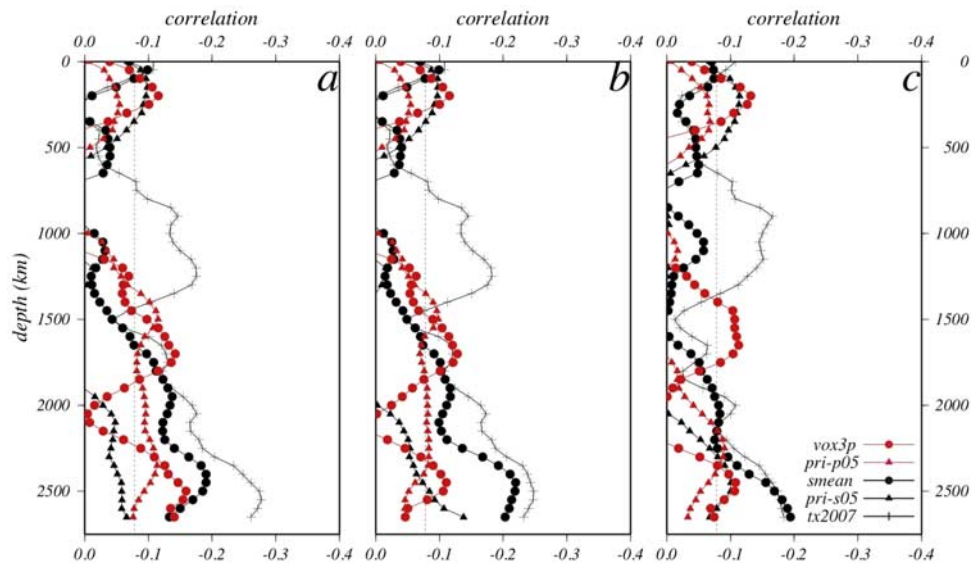


**Figure 12.** Correlations up to harmonic degree 20 between the horizontal gradients of tomographic models and 44 advected plume conduits modeled according to SA06 (a) in the moving-source hypothesis and (b) in the fixed-source hypothesis and (c) the same 44 plumes, assumed vertical under the corresponding hot spots. Symbols are as in Figure 9. The 90% significance level corresponding to a degree 20 harmonic parameterization ( $21^2$  coefficients) is shown (dashed, vertical lines).

### 3.2.3. Correlation Between Plumes and the Horizontal Gradient of Tomographic Models

[38] *Thorne et al.* [2004] show that the surface locations of *Steinberger's* [2000] hot spots (Figure 6) have a tendency to lie in regions where lowermost-mantle seismic anomalies vary quickly in the horizontal direction: maxima of the tomographic models' horizontal gradient. Their observation was not based on a formal calculation of correlation, which we conduct here. From the spherical harmonic expansions of all considered tomographic models (both positive and negative anomalies), tapered as above with a cosine-squared filter, we compute their horizontal gradients as functions of longitude and latitude and at all depths. We then follow the procedure described above to calculate the correlation  $r$  between gradient amplitude and plume-conduit distribution (Figure 12).

[39] Correlations in Figure 12 are low at most mantle depths, and often below significance, both in the advected- (Figures 12a and 12b) and vertical-plume (Figure 12c) hypotheses, and regardless of whether plume sources are assumed to be moving (Figure 12a), or fixed to their initial location (Figure 12b). They are generally lower than those for slow seismic anomalies in Figure 9, with the exception of the very bottom of the mantle, where

the horizontal gradients of models *smean* and *tx2007* are better correlated with vertical plumes (Figure 12c) than the corresponding seismic velocity anomalies (Figure 9b).

[40] We thus partly reproduce the observation of *Thorne et al.* [2004], who considered a different, earlier family of tomographic models. However, as noted by *Thorne et al.* [2004] themselves, their proposed mechanism of plume origin close to high gradients of tomography at the base of the mantle has the drawback of neglecting the effects of mantle advection. Comparing Figure 12a or 12b with Figure 9a, it is clear that dynamically modeled, advected plumes with moving sources are correlated with seismic anomalies much better than they are correlated with the horizontal gradient of seismic anomalies, both in the moving-source and fixed-source hypotheses.

[41] To reconcile *Thorne et al.'s* [2004] mechanism with our findings, one could hypothesize that plumes initially form close to high gradients near the edges of thermochemical piles [*McNamara and Zhong, 2005; Torsvik et al., 2006*], but their sources are subsequently advected to, and are now mostly located in regions of slow seismic anomalies.

[42] The work of *Torsvik et al.* [2006] suggests that the picture might change when one attempts to correlate the locations of large igneous provinces

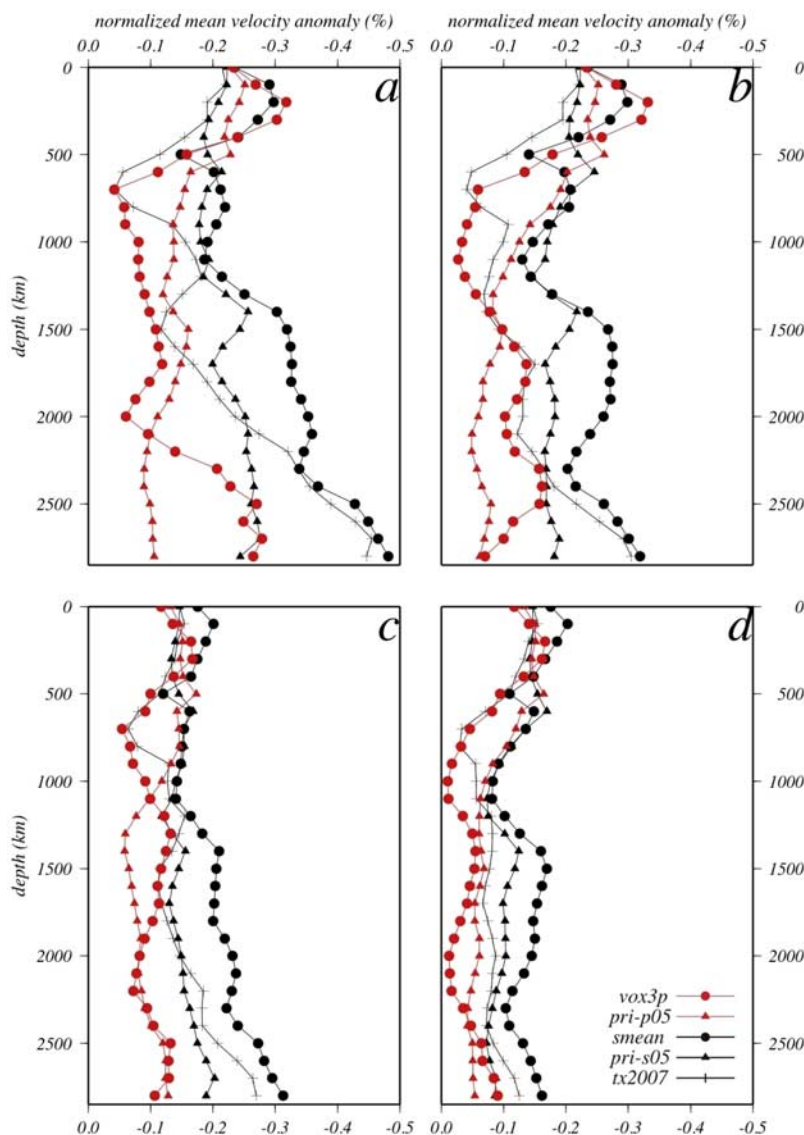


**Figure 13.** We mask tomographic models with (a) 12 advectioned plumes selected by SA06, (b) the same 12 plumes, assumed vertical under the corresponding hot spots, (c) 44 advectioned plumes (including the original 12), and (d) the same 44 plumes, assumed vertical. Plotted values are mean velocity anomalies within plumes, normalized by their maximum at each depth, from all considered *P* and *S* models. Colors, symbols, and line styles are as in Figure 9.

(presumably indicative of the arrival of a plume head with a strong conduit source), rather than those of all hot spots, with seismic velocity gradients. This will be the subject of future work; our initial results indicate that, similar to surface hot spot locations, reconstructed large igneous provinces are significantly correlated with gradients only for models *smean* and *tx2007*, near the base of the mantle.

### 3.3. Masking Seismic Anomalies With Dynamic Plume-Conduit Models

[43] For each tomographic model, we normalize velocity anomalies at each depth by their maxi-

um value at that depth. We then set to zero (“mask”) the resulting normalized images outside dynamic models of plume conduits. We calculate, and show in Figure 13, the mean values taken at each depth by masked normalized images.

[44] Figure 13 shows that, on average, tomographically mapped velocities are negative at presumed plume locations at all depths in the mantle. This is in agreement with Figure 9, proving that the properties of harmonic-based correlations do not distort our observations in section 3.2.

[45] Comparing Figure 13a with 13b, or Figure 13c with 13d, we also see that neglecting plume ad-

vection and the subsequent variability of modeled plume shapes results in a loss of consistency with tomographic images throughout the lower mantle: this further substantiates the findings of *Steinberger and O'Connell* [1998] and *Steinberger* [2000]. Comparing Figure 13a with 13c, or Figure 13b with 13d, we find that average seismic velocities mapped at plume locations are lower, if only a limited number of plumes, of likely deep-mantle origin, are considered. This is in agreement with the idea that only a small subset of hot spots originate from deep mantle plumes [*Courtillot et al.*, 2003]. This effect might be enhanced by optimizing our selection of presumed deep-mantle plumes: for instance some hot spots that we and SA06 treat as originated by deep-mantle plumes, are listed as “secondary” or “tertiary” by *Courtillot et al.* [2003]. We shall explore this issue in future work.

### 3.4. Analysis of Individual Hot Spots

[46] Following *Courtillot et al.* [2003], we make use of the tools assembled in this work to quantify each hot spot's likelihood of having a deep mantle origin. In practice, we introduce at each grid point within a modeled advected plume a binary quantity that equals 1 if the masked, normalized velocity anomaly at that location is negative and its absolute value  $>0.15\%$ , 0 otherwise. This value is then integrated along the plume, and the result normalized by the number of grid points sampled by the plume. If the result is close to 1, we infer that a deep mantle origin for the hot spot in question is consistent with tomography. It is understood that this analysis is not sufficient to determine whether the hot spot is the surface expression of a narrow plume, or part of a more complex system, with plumes merging at some depth into large-scale slow/hot provinces.

[47] We repeat this exercise for each dynamically modeled plume, and for all considered tomographic models. For each plume, we average the normalized vertical extent as measured from all tomographic models. The results are shown in Figure 14. A considerable agreement is found between tomographic images in attributing a large vertical extent to a significant subset of plumes (top of Figure 14). Of the 12 hot spots associated by Figure 14 to deepest Earth structure, 5 correspond to plumes that *Courtillot et al.* [2003] also find likely to be primary: Reunion, Samoa, Iceland, Hawaii, Tristan. According to Figure 14, the remaining 4 primary plumes of *Courtillot et al.* [2003] are either imaged very differently by different tomographic models

(Caroline, Easter), or likely to be short (Louisville). We have neglected Afar here, but a visual analysis of Figures 3, 4, 7 and 8 suggests that a narrow slow anomaly associated with that hot spot extends coherently from the upper into the lowermost mantle, with an advected conduit of shape similar to that modeled at East Africa.

## 4. Conclusions

[48] Our quantitative plume-detection experiment and our evaluation of agreement between seismic and geodynamic results show the following:

[49] 1. A deep mantle origin is plausible, perhaps likely, for a *limited* number of hot spots, but unlikely for most at current seismic resolution.

[50] 2. Most slow, narrow, and vertically coherent (plume-like) features extending to large depths in tomographic models are found under either the southern central part of the Pacific Ocean or southern/northwestern Africa and the neighboring oceans.

[51] 3. A plume model that accounts for plume tilt caused by mantle flow [SA06] is better correlated with tomographic results than a model of purely vertical plumes.

[52] 4. The correlation between moving-source advected plume models and tomographic results is higher than the correlation between vertical (or fixed-source advected) plume models and the horizontal gradients of tomographic models.

[53] What is then the mechanism by virtue of which hot mantle material rises to form hot spots? *Courtillot et al.* [2003] make a distinction between (1) primary hot spots, or hot spots of deep mantle origin, to each of which a single, narrow hot spot plume must be associated; (2) secondary hot spots, originating from the top of a slow/hot province; and (3) tertiary hot spots, or those of lithospheric origin. On the basis of point 2 (paragraph 50) one would favor a picture of the Earth's mantle where large-scale slow/hot regions act as “plume farms” for secondary hot spots. This would partly explain the results of Reif and Williams (manuscript in preparation, 2007), and Figure 1 here, associating the anomalously large scale length of slow anomalies in the lowermost mantle to large-scale slow/hot provinces [*Courtillot et al.*, 2003, Figure 4].

[54] There are, however, several pieces of evidence to advocate the primary-plume concept. In the first place, we find the Icelandic hot spot, clearly not



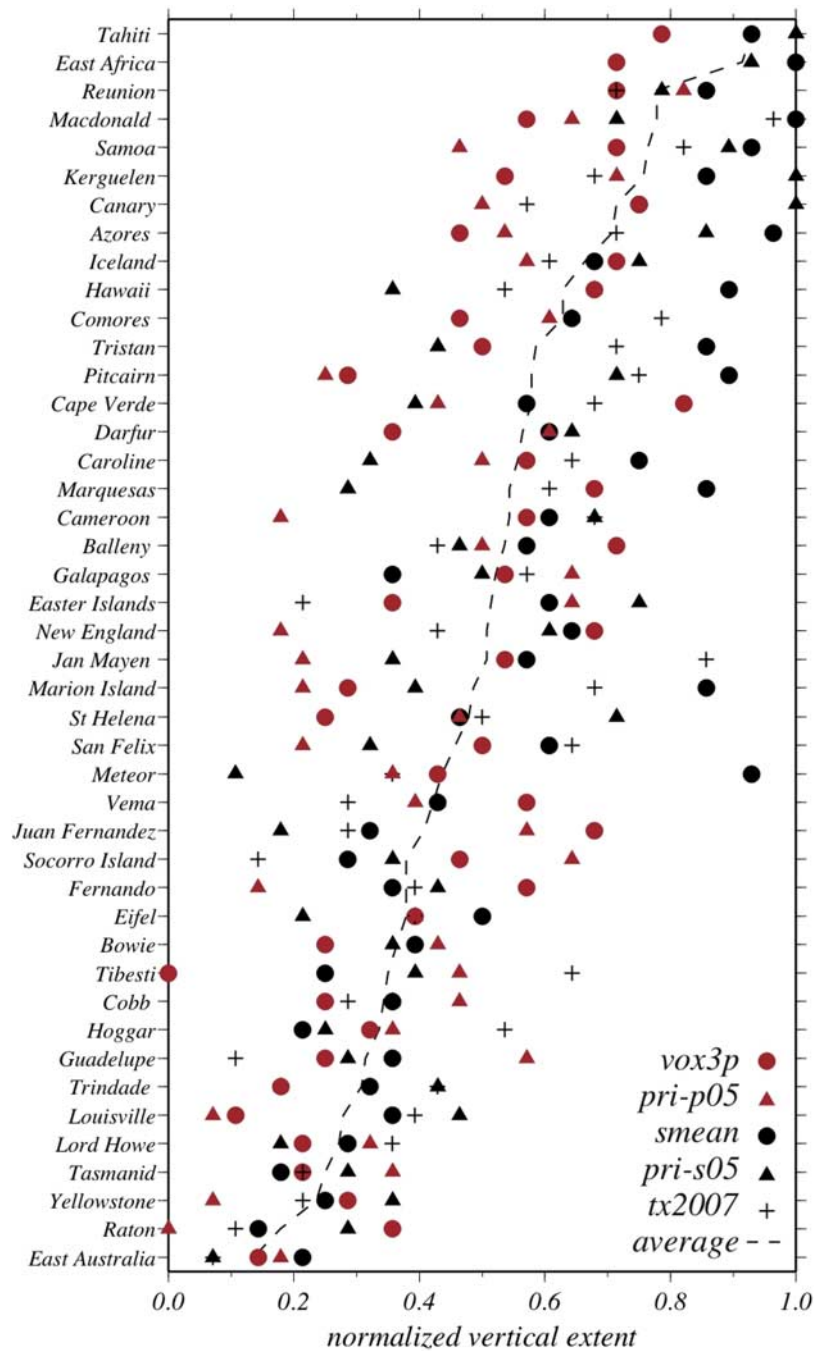


**Figure 14.** Vertical extent of coherent slow anomalies found at modeled, advected plume conduits, normalized by plume length, found from the seismic *S* (black symbols) models *smean* (black circles), *pri-s06* (black triangles), and *tx2007* (black crosses), and *P* (red symbols) models *vox3p* (red circles) and *pri-p05* (red triangles). We sorted all modeled plumes on the basis of the averages (dashed line) of values found from all seismic models: hot spots at the top of the plot are the most likely to have deep mantle origin, while the ones at the bottom must probably be associated to shallow-Earth phenomena.

associated with either large-scale low velocity province in the lowermost-mantle, to have likely deep mantle origin (Figure 14), confirmed by *Courtillot et al.* [2003]. In the second place,

*Schubert et al.* [2004] contend that the geographic distribution of detected plumes is better explained by the presence of clusters of close but separate narrow plumes (“plume forests”) than by the

superplume model of *Courtilot et al.* [2003]. Last, in a “plume-farm” regime, the pattern of seismic heterogeneity in the lower mantle would be dominated by large, slow domes: this is in contrast with the significant correlation we find between tomography and modeled narrow plumes (point 3 above).

[55] The latter argument, that high correlation between tomography and advected plumes is evidence for primary-plume hot spot formation, is partly circular, since our primary-plume model relies on a model of mantle flow based on tomography: modeled large-scale upwellings, toward which modeled plume sources are advected, tend by construction to overlay large-scale slow tomographic anomalies in the lowermost mantle. On the other hand, one would expect that, were hot spots of mostly secondary origin, advected and vertical modeled plume conduits would be equally lost in the large-scale slow regions of the lowermost mantle, and the significant correlation change we see in Figures 9, 10 and 13, reflecting a resemblance between modeled plume sources and smaller-scale anomalies at the base of the mantle, would not be possible.

[56] The simplest picture to then accommodate such a variety of diverging indications is one of co-existing primary and secondary plumes, with different mechanisms of mantle upwelling active in different regions of the Earth.

## Acknowledgments

[57] We thank Shijie Zhong, Christine Reif, and Jean-Paul Montagner for several useful discussions. Peter van Keken and two anonymous reviewers provided additional comments. We thank all the authors of analyzed tomographic models for sharing all model information. L.B. thanks Domenico Giardini for his constant support and encouragement. All tomographic model coefficients in our spherical harmonic format, and software to interpret them, are available through the SPICE Web site: <http://www.spice-rtn.org/research/planetaryscale/tomography/>.

## References

- Anderson, D. L. (1998), The edges of the mantle, in *The Core-Mantle Boundary Region*, *Geodyn. Ser.*, vol. 28, edited by M. E. Gurnis, E. K. Wysession, and B. A. Buffett, pp. 255–271, AGU, Washington, D. C.
- Anderson, D. L. (2000), The thermal state of the upper mantle: No role for mantle plumes, *Geophys. Res. Lett.*, *27*, 3623–3626.
- Antolik, M., G. Ekström, and A. M. Dziewonski (2001), Global event location with full and sparse data sets using three-dimensional models of mantle P-wave velocity, *Pure Appl. Geophys.*, *158*, 291–317.
- Becker, T., and L. Boschi (2002), A comparison of tomographic and geodynamic mantle models, *Geochem. Geophys. Geosyst.*, *3*(1), 1003, doi:10.1029/2001GC000168.
- Bijwaard, H., W. Spakman, and E. R. Engdahl (1998), Closing the gap between regional and global travel time tomography, *J. Geophys. Res.*, *103*, 30,055–30,078.
- Boschi, L. (2003), Measures of resolution in global body wave tomography, *Geophys. Res. Lett.*, *30*(19), 1978, doi:10.1029/2003GL018222.
- Boschi, L. (2006), Global multiresolution models of surface wave propagation: Comparing equivalently regularized Born and ray theoretical solutions, *Geophys. J. Int.*, *167*, 238–252.
- Boschi, L., and A. Dziewonski (1999), High- and low-resolution images of the Earth’s mantle: Implications of different approaches to tomographic modeling, *J. Geophys. Res.*, *104*, 25,567–25,594.
- Boschi, L., T. W. Becker, G. Soldati, and A. M. Dziewonski (2006), On the relevance of Born theory in global seismic tomography, *Geophys. Res. Lett.*, *33*, L06302, doi:10.1029/2005GL025063.
- Clouard, V., and A. Bonneville (2001), How many Pacific hotspots are fed by deep-mantle plumes?, *Geology*, *21*, 695–698.
- Courtilot, V., A. Davaille, J. Besse, and J. Stock (2003), Three distinct types of hotspots in the Earth’s mantle, *Earth Planet. Sci. Lett.*, *205*, 295–308.
- Dahlen, F. A., and G. Nolet (2005), Comment on “On sensitivity kernels for ‘wave-equation’ transmission tomography” by de Hoop and van der Hilst, *Geophys. J. Int.*, *163*, 949–951.
- Davaille, A. (1999), Simultaneous generation of hotspots and superswells by convection in a heterogeneous planetary mantle, *Nature*, *402*, 756–760.
- Davaille, A., F. Girard, and M. Le Bars (2002), How to anchor hotspots in a convecting mantle?, *Earth Planet. Sci. Lett.*, *203*, 621–634.
- Davies, G. F. (1988), Ocean bathymetry and mantle convection: 1. Large-scale flow and hotspots, *J. Geophys. Res.*, *93*, 10,467–10,480.
- Davies, G. F. (2005), A case for mantle plumes, *Chin. Sci. Bull.*, *50*, 1541–1554.
- de Hoop, M. V., and R. D. van der Hilst (2005a), On sensitivity kernels for ‘wave-equation’ transmission tomography, *Geophys. J. Int.*, *160*, 621–633.
- de Hoop, M. V., and R. D. van der Hilst (2005b), Reply to comment by F. A. Dahlen and G. Nolet on “On sensitivity kernels for ‘wave-equation’ transmission tomography,” *Geophys. J. Int.*, *163*, 952–955.
- Foulger, G. R. (2002), Plumes or plate tectonic processes, *Astron. Geophys.*, *43*, 19–23.
- Foulger, G. R., J. H. Natland, and D. L. Anderson (2005), Genesis of the Iceland anomaly by plate tectonic processes, in *Plates, Plumes, and Paradigms*, edited by G. R. Foulger et al., *Spec. Pap. Geol. Soc. of Am.*, *388*, 595–625.
- Gaherty, J. B. (2001), Seismic evidence for hotspot-induced buoyant flow beneath the Reykjanes Ridge, *Science*, *293*, 1645–1647.
- Goes, S., F. Cammarano, and U. Hansen (2004), Synthetic signature of thermal mantle plumes, *Earth Planet. Sci. Lett.*, *218*, 403–419.
- Grand, S. P. (1994), Mantle shear structure beneath the Americas and the surrounding oceans, *J. Geophys. Res.*, *99*, 11,591–11,621.

- Grand, S. P., R. D. van der Hilst, and S. Widiyantoro (1997), Global seismic tomography: A snapshot of convection in the Earth, *GSA Today*, *7*, 1–7.
- Jellinek, A. M., and M. Manga (2002), The influence of a chemical boundary layer on the fixity, spacing and lifetime of mantle plumes, *Nature*, *418*, 760–763.
- Ji, Y., and H.-C. Nataf (1998a), Detection of mantle plumes in the lower mantle by diffraction tomography: Theory, *Earth Planet. Sci. Lett.*, *159*, 87–98.
- Ji, Y., and H.-C. Nataf (1998b), Detection of mantle plumes in the lower mantle by diffraction tomography: Hawaii, *Earth Planet. Sci. Lett.*, *159*, 99–115.
- Labrosse, S. (2002), Hotspots, mantle plumes and core heat loss, *Earth Planet. Sci. Lett.*, *199*, 147–156.
- Masters, G., H. Bolton, and G. Laske (1999), Joint seismic tomography for P and S velocities: How pervasive are chemical anomalies in the mantle?, *Eos Trans. AGU*, *80*(17), Spring Meet. Suppl., S14.
- McNamara, A. K., and S. Zhong (2004), The influence of thermochemical convection on the fixity of mantle plumes, *Earth Planet. Sci. Lett.*, *222*, 485–500.
- McNamara, A. K., and S. Zhong (2005), Thermochemical structures beneath Africa and the Pacific Ocean, *Nature*, *437*, 1136–1139.
- McNutt, M. K. (1998), Superswells, *Rev. Geophys.*, *36*, 211–244.
- Montagner, J.-P. (1994), Can seismology tell us anything about convection in the mantle?, *Rev. Geophys.*, *32*, 115–137.
- Montagner, J.-P., and J. Ritsema (2001), Interactions between ridges and plumes, *Science*, *294*, 1472–1473.
- Montelli, R., G. Nolet, F. A. Dahlen, G. Masters, E. R. Engdahl, and S.-H. Hung (2004a), Finite-frequency tomography reveals a variety of plumes in the mantle, *Science*, *303*, 338–343.
- Montelli, R., G. Nolet, G. Masters, F. A. Dahlen, and S.-H. Hung (2004b), Global P and PP traveltime tomography: Rays versus waves, *Geophys. J. Int.*, *158*, 637–654.
- Montelli, R., G. Nolet, and F. A. Dahlen (2006a), Comment on “Banana-doughnut kernels and mantle tomography” by van der Hilst and de Hoop, *Geophys. J. Int.*, *167*, 1204–1210.
- Montelli, R., G. Nolet, F. A. Dahlen, and G. Masters (2006b), A catalogue of deep mantle plumes: New results from finite-frequency tomography, *Geochem. Geophys. Geosyst.*, *7*, Q11007, doi:10.1029/2006GC001248.
- Morgan, W. J. (1971), Convection plumes in the lower mantle, *Nature*, *230*, 42.
- Morgan, W. J. (1978), Rodriguez, Darwin, Amsterdam, . . . , a second type of hotspot island, *J. Geophys. Res.*, *83*, 5355–5360.
- Nataf, H.-C. (2000), Seismic imaging of mantle plumes, *Annu. Rev. Earth Planet. Sci.*, *28*, 391–417.
- Nyblade, A. A., and S. W. Robinson (1994), The African superswell, *Geophys. Res. Lett.*, *21*, 765–768.
- Press, W. H., S. A. Teukolsky, W. T. Vetterling, and B. P. Flannery (1994), *Numerical Recipes in Fortran*, Cambridge University Press, Cambridge, U. K.
- Qin, Y., Y. Capdeville, V. Maupin, J.-P. Montagner, and L. Boschi (2007), Inversion of SPICE benchmark dataset and test of global tomographic models, *Geophys. Res. Abstr.*, *9*, 05064.
- Ray, T. W., and D. L. Anderson (1994), Spherical disharmonics in the Earth sciences and the spatial solution: Ridges, hotspots, slabs, geochemistry, and tomography correlations, *J. Geophys. Res.*, *99*, 9605–9614.
- Ritsema, J., H. J. van Heijst, and J. H. Woodhouse (1999), Complex shear wave velocity structure imaged beneath Africa and Iceland, *Science*, *286*, 1925–1928.
- Schubert, G., G. Masters, P. Olson, and P. Tackley (2004), Superplumes or plume clusters?, *Phys. Earth Planet. Inter.*, *146*, 147–162.
- Seidler, E., W. R. Jacoby, and H. Cavaşak (1999), Hotspot distribution, gravity, mantle tomography: Evidence for plumes, *J. Geodyn.*, *27*, 585–608.
- Simmons, N. A., A. M. Forte, and S. P. Grand (2006), Constraining mantle flow with seismic and geodynamic data: A joint approach, *Earth Planet. Sci. Lett.*, *46*, 109–124.
- Sleep, N. H. (1990), Hotspots and mantle plumes: Some phenomenology, *J. Geophys. Res.*, *95*, 6715–6736.
- Sleep, N. H. (2002a), Ridge-crossing mantle plumes and gaps in tracks, *Geochem. Geophys. Geosyst.*, *3*(12), 8505, doi:10.1029/2001GC000290.
- Sleep, N. H. (2002b), Local lithospheric relief associated with fracture zones and ponded plume material, *Geochem. Geophys. Geosyst.*, *3*(12), 8506, doi:10.1029/2002GC000376.
- Sleep, N. H. (2006), Mantle plumes from top to bottom, *Earth Sci. Rev.*, *77*, 231–271.
- Steinberger, B. (2000), Plumes in a convecting mantle: Models and observations for individual hotspots, *J. Geophys. Res.*, *105*, 11,127–11,152.
- Steinberger, B., and M. Antretter (2006), Conduit diameter and buoyant rising speed of mantle plumes: Implications for the motion of hot spots and shape of plume conduits, *Geochem. Geophys. Geosyst.*, *7*, Q11018, doi:10.1029/2006GC001409.
- Steinberger, B., and A. R. Calderwood (2006), Models of large-scale viscous flow in the Earth’s mantle with constraints from mineral physics and surface observations, *Geophys. J. Int.*, *167*, 1461–1481.
- Steinberger, B., and R. J. O’Connell (1998), Advection of plumes in mantle flow: Implications for hotspot motion, mantle viscosity and plume distribution, *Geophys. J. Int.*, *132*, 412–434.
- Tackley, P. J. (2002), Strong heterogeneity caused by deep mantle layering, *Geochem. Geophys. Geosyst.*, *3*(4), 1024, doi:10.1029/2001GC000167.
- Thorne, M. S., E. J. Garnero, and S. P. Grand (2004), Geographic correlation between hot spots and deep mantle lateral shear-wave velocity gradients, *Phys. Earth Planet. Inter.*, *146*, 47–63.
- Torsvik, T. H., M. A. Smethurst, K. Burke, and B. Steinberger (2006), Large igneous provinces generated from the margins of the large low-velocity provinces in the deep mantle, *Geophys. J. Int.*, *167*, 1447–1460, doi:10.1111/j.1365-246X.2006.03158.x.
- Trampert, J., and J. Spetzler (2006), Surface wave tomography: Finite-frequency effects lost in the null space, *Geophys. J. Int.*, *164*, 394–400.
- Turcotte, D. L., and E. R. Oxburgh (1973), Mid-plate tectonics, *Nature*, *244*, 337–339.
- van der Hilst, R. D., and M. V. de Hoop (2005), Banana-doughnut kernels and mantle tomography, *Geophys. J. Int.*, *163*, 956–961.
- van der Hilst, R. D., and M. V. de Hoop (2006), Reply to comment by R. Montelli, G. Nolet and F. A. Dahlen on “Banana-doughnut kernels and mantle tomography,” *Geophys. J. Int.*, *167*, 1211–1214.
- van der Hilst, R. D., S. Widiyantoro, and E. R. Engdahl (1997), Evidence for deep mantle circulation from global tomography, *Nature*, *386*, 578–584.
- Wen, L., and D. L. Anderson (1997), Slabs, hotspots, cratons and mantle convection revealed from residual seismic tomography in the upper mantle, *Phys. Earth Planet. Inter.*, *99*, 131–143.

Zhong, S. (2006), Constraints on thermochemical convection of the mantle from plume heat flux, plume excess temperature, and upper mantle temperature, *J. Geophys. Res.*, *111*, B04409, doi:10.1029/2005JB003972.

Zhong, S., M. T. Zuber, L. Moresi, and M. Gurnis (2000), Role of temperature-dependent viscosity and surface plates in spherical shell models of mantle convection, *J. Geophys. Res.*, *105*, 11,063–11,082.